LEGIBILITY NOTICE

A major purpose of the Technical Information Center is to provide the broadest dissemination possible of information contained in DOE's Research and Development Reports to business, industry, the academic community, and federal, state and local governments.

Although a small portion of this report is not reproducible, it is being made available to expedite the availability of information on the research discussed herein.

Los Alamos National Laboratory is operated by the University of California for the United States Department of Energy under contract W-7405-ENG-36

LA-UR--88-97

DE88 005378

TITLE: INTERMEDIATE ENERGY NEUTRINO PHYSICS

AUTHOR(S): D. Hywel White, MP-4

SUBMITTED TO: TASI-87 Proceedings, Santa Fe, NM
July 1987

DISCLAIMER

Los Alamos National Laboratory
Los Alamos, New Mexico 87545

FORM NO. 836 (R4
ST. NO. 2629 5/81

INTERMEDIATE ENERGY NEUTRINO PHYSICS

D. Hywel White
Los Alamos National Laboratory
Los Alamos, NM

Occasionally, our understanding of a situation in physics is apparently so clear that consequences of a particular experimental result can imply a substantial confrontation with our view of the physical world. The standard model of electroweak interactions is now so clear that a number of experimental consequences are precisely predicted. This seems like a delightful situation for experimenters, but the bad news is that the experiments on which the predictions rest are at least hard and certainly expensive. We will focus on one such an experiment in this talk; the principal goal of the experiment was to measure neutrino - electron scattering, and also to measure a number of other exclusive channels in neutrino scattering which have bearing on our view of hadronic electroweak interactions.

We start with the known leptons, arranged in three families as shown below

$$\nu_e \qquad \nu_\mu \qquad \nu_\tau$$

$$e \qquad \mu \qquad \tau \ .$$

We expect that charged-current interactions only cause transitions within the same family and are universal. The neutral-reaction current on the other hand is given by

$$I_{3w} \ + \ 2Q\sin^2\theta_W \ .$$

Where I_{3w} is the weak isospin $\pm 1/2$ derived from the position in the family.

It is remarkable that the couplings to the quarks are the same as the leptons in the standard model; of course this prediction is not amenable to a totally clean test but is nevertheless accessible indirectly, for example through the elastic-scattering reaction

$$\nu_\mu \ p \ \rightarrow \ \nu_\mu \ p \ .$$

The experimental program described here is also designed to measure this reaction.

Muon-neutrino electron scattering is described by the diagram in Fig. 1 and without one-loop corrections the cross section is given by

$$\sigma \ = \ G^2 \ m_e \ E_\nu / 2\pi \ [(1 \ - \ 2 \sin^2\theta_W)^2 \ + \ 4/3 \ \sin^4\theta_W]$$

Neutrino - Electron Scattering

$$\nu_\mu + e \rightarrow \nu_\mu + e$$

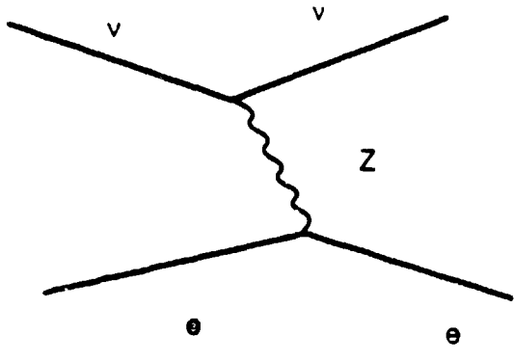

Figure 1

It turns out that direct radiative corrections are negligible in this reaction due to the cancellation of principal radiative corrections at the one-loop level in the standard model.

The experimental signature for neutrino-electron scattering is minimal, perhaps unfortunately simple, just a recoil electron, because the incoming neutrino is invisible. The neutrino-scattering cross section is proportional to the energy in the c.m. system and so the small mass of the electron is a decided disadvantage. The nucleon-to-electron mass ratio implies that by far a greater number of events will come when nucleons are target particles and so the experiment must discriminate against these events. A positive feature of the low electron mass is that the recoil angle of the electron is small; in fact the angle is bounded by

$$\theta_e < \sqrt{(2m_e/E_e)} \quad .$$

The experimental strategy then is to look for events peaked in the forward direction in which the forward-going particle looks like an electromagnetic shower. Not only can we use these positive characteristics of the event but we can demand that there be nothing else going on in the event and discriminate against relatively busy hadronic events.

The cross section is small (10^{-42} cm^2) and so the detector must be big to get enough events. The detector must be able to measure angle well, and be able to tell electrons from other particles. To separate events from occurrences at random times the detector must also measure time well.

It is well known that experiments of this type are not done by any person working alone. We are listed below.

Leif Ahrens, Sam Aronson, Bruce Gibbard, Mike Murtagh, Steve Murtagh, Hywel White*	Brookhaven National Laboratory
John Callas, Dave Cutts, Milind Diwan, Jan Hoftun, Bob Lanou	Brown University
Yoshi Kurihara	Hiroshima University
Kazuo Abe, Katsuya Amako, Seiji Kabe, Takao Shinkawa, Susumu Terada	KEK
Yori Nagashima, Yoichiro Suzuki, Shuji Tatsumi, Keigo Yamaguchi	Osaka University
Mike Marx, Dave Hedin, Eric Stern	Stonybrook
Gene Beier, Rick van Berg, Stan Durkin, Max Heagy, Mike Hurley, Al Mann, Mitch Newcomer, Brig Williams, Tom York	University of Pennsylvania

*Presently at Los Alamos National Laboratory.

The experiment used liquid scintillator as a target medium in acrylic cells with phototubes at each end. This means that the detector is almost entirely active (> 85%) so that any energy deposition is visible in the device. The detector is a total absorption calorimeter, so that energy is measured well, and the liquid scintillator ensures that the time of events is also measured well, to about 2ns. Between the scintillators there are drift tubes that are used to measure the position at which the particles cross the plane of the device and because these cells are 150 mm apart this results in an angular resolution of about 10 mr. At 1 GeV the maximum angle of the recoil electron is 30 mr. Figure 2 shows a diagram of the detector as a whole. In Fig. 3 we show a part of the detector with calorimeter cells indicated and proportional drift tubes (PDT) in between. The calorimeter cells are made with acrylic tubes in which the light from the scintillator is transmitted to the end of the cell by total internal reflection on the outside surface of the acrylic. It would be prohibitively expensive to polish the surface of the acrylic as is usually done with scintillators but we found that the same process as is used in making supermarket signs, namely to extrude the acrylic through a special die, will do very well. This is partly because the striations that are left by the extrusion process are along the length of the tube and do not hinder the reflection of the light in that general direction much at all. In

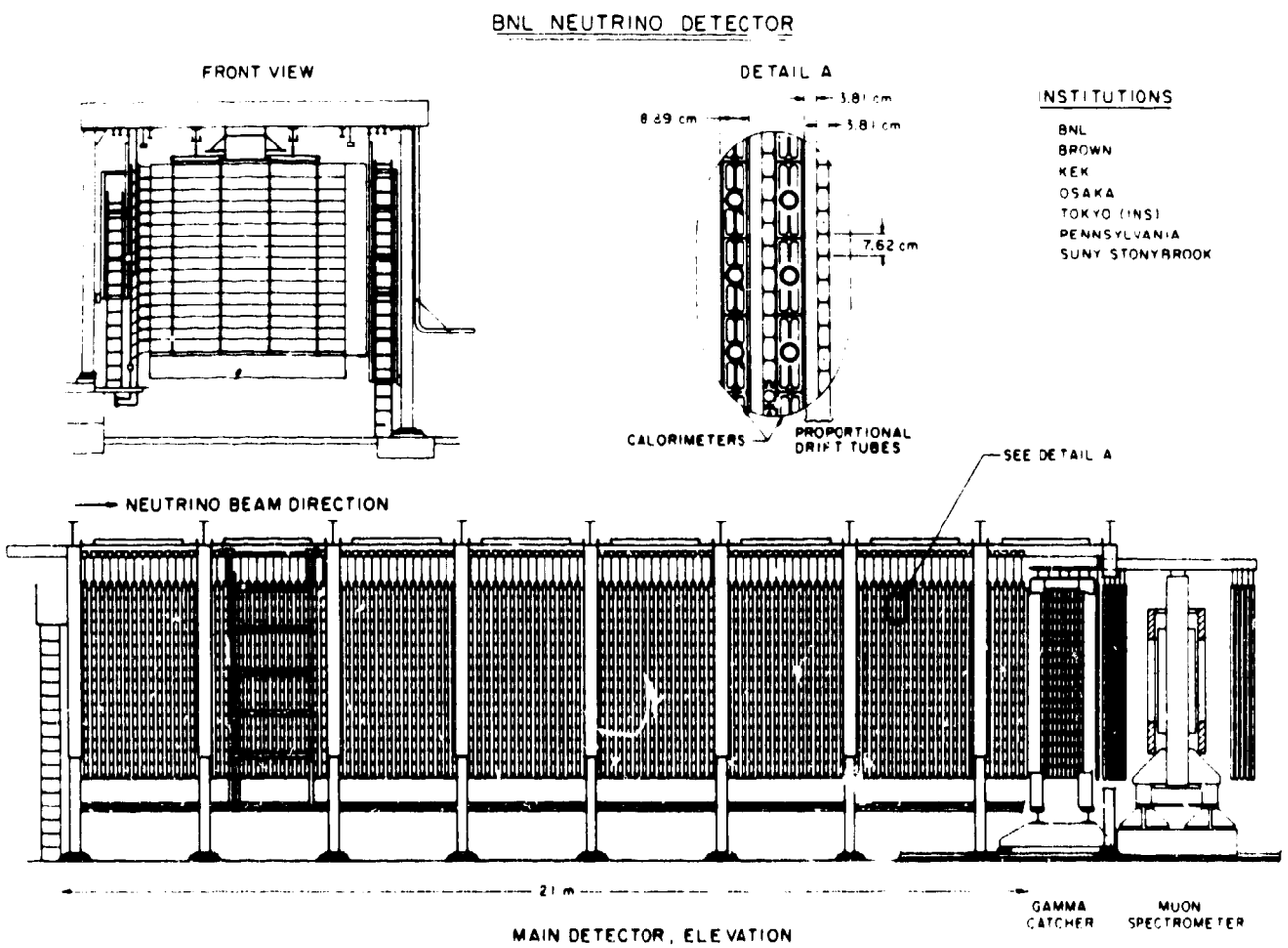
BNL NEUTRINO DETECTOR
FRONT VIEW
DETAIL A
3.81 cm
8.89 cm
3.81 cm
7.62 cm
CALORIMETERS
PROPORTIONAL DRIFT TUBES
INSTITUTIONS
BNL
BROWN
KEK
OSAKA
TOKYO (INS)
PENNSYLVANIA
SUNY STONYBROOK
SEE DETAIL A
NEUTRINO BEAM DIRECTION
21 m
GAMMA CATCHER
MUON SPECTROMETER
MAIN DETECTOR, ELEVATION

Figure 2

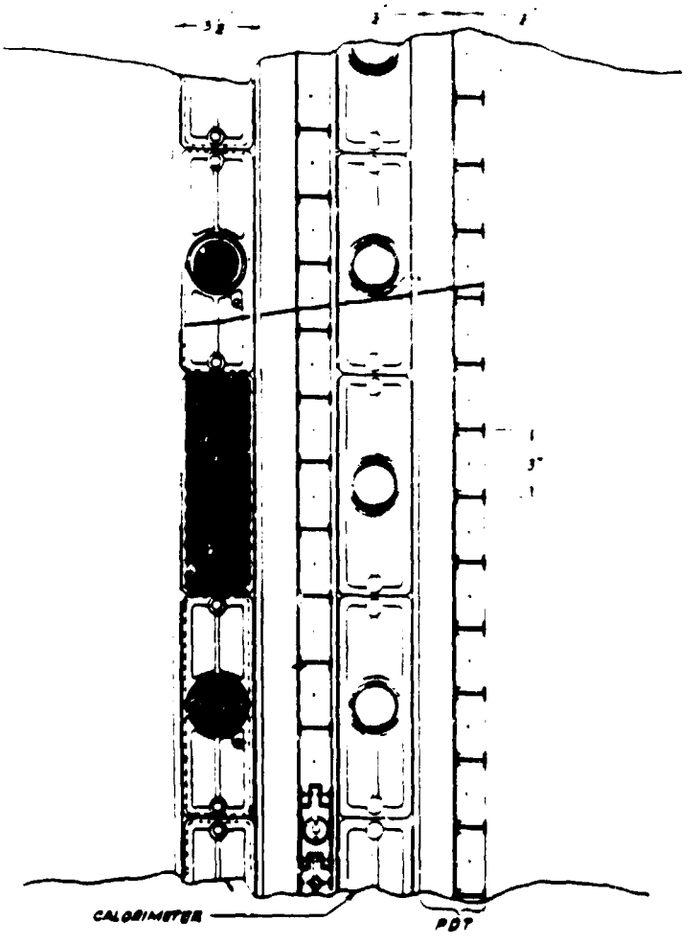

Figure 3

contrast, the reflectivity in a direction perpendicular to this is relatively poor, but we don't care. The ends of the tubes are sawn off during the extrusion process and afterwards the end caps are glued on. It turns out that this is a tricky game because the acrylic exhibits strange behavior in releasing the considerable strains in the material from the extruding process. There is a little black magic involved in the successful bonding of the end caps to the tubes so that joints remain secure over the lifetime of the experiment. The cells need to be light tight of course, so they are covered individually with black plastic after the end caps have been bonded and the joint tested. The acrylic cells when full of liquid scintillator will only support about a four-foot head of liquid pressure. The cells are arranged in a wall supported by stainless steel straps as shown in Fig. 4. If these cells are filled from a single manifold, destruction will result, as was experimentally determined on one occasion. The solution to this problem is to fill each cell independently so that the internal pressure of each cell is close to atmospheric pressure. The cells were flexible enough to deal with the overall variation of atmospheric pressure from the weather.

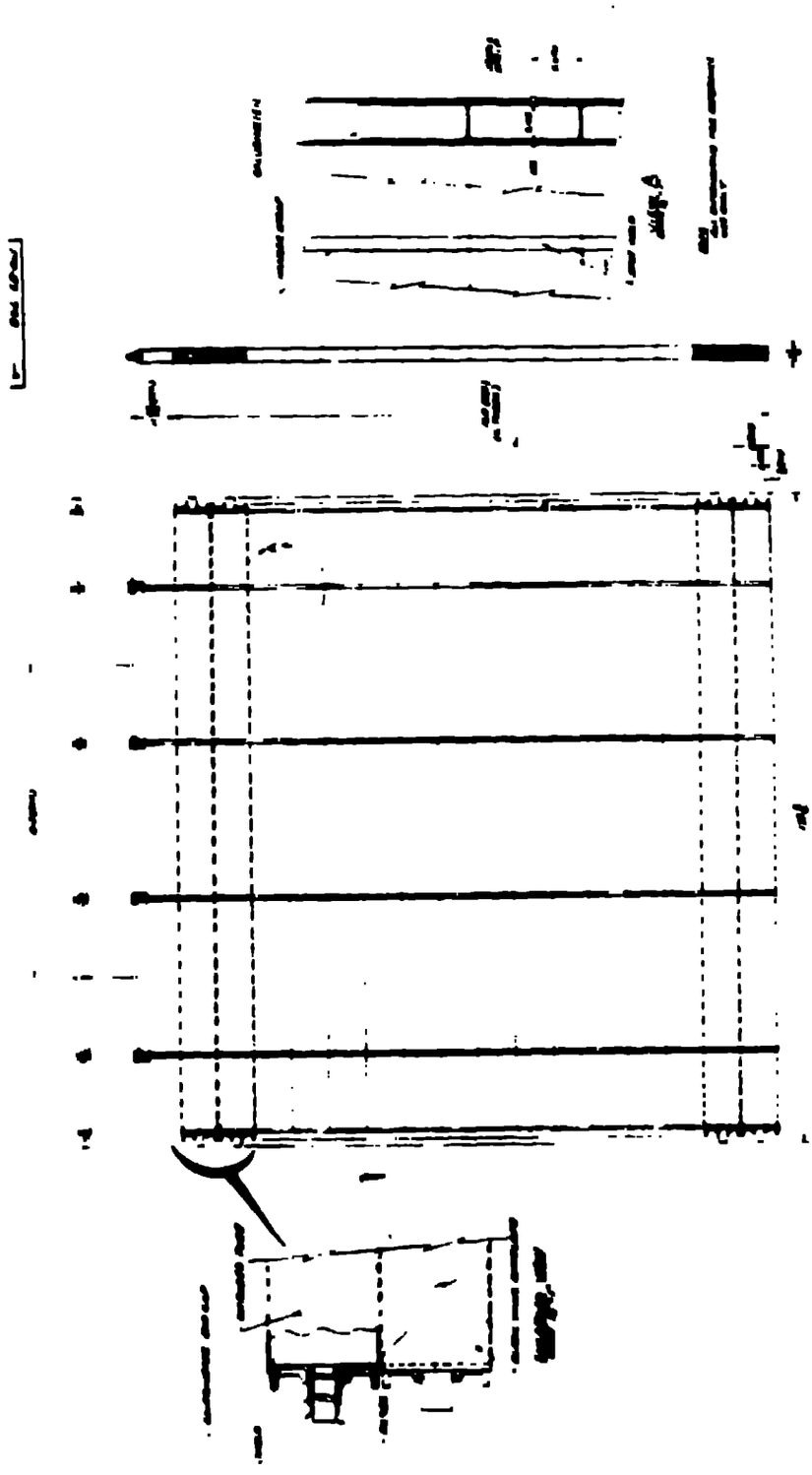

Figure 4

The proportional drift tubes consist of a number of cells 3" x 1.5" in cross section with a 3 mil stainless steel wire in the center of the cell. The assembly is shown in Fig. 5. The wire is maintained at a potential of about 2 kV so that the electrons from the ion pairs produced in the gas of the chamber when a particle passes through are multiplied in the vicinity of the wire. The array of cells is made relatively precisely by gluing flat aluminum sheets to parallel I-beams made out of roll-formed thin aluminum. In this way a low cost pair of chambers is made so that the pair of chambers gives a measure of the traversing particle position to about a millimeter in two dimensions over an area of about 4 m × 4 m. It is important to keep the gas gain of the PDT's constant and this was accomplished by measuring the pulse-height spectrum from an x-ray source in an identical small chamber in the same gas stream. The high voltage was varied under computer control so that the peak position was maintained constant. These are a few of the methods that were used in this experiment to ensure that a large massive piece of apparatus was available that would reconstruct particle positions at a large number of points along a track and to measure the ionization loss in the cells that were traversed by the particle. The granularity of the detector was of paramount importance and eventually was really limited by financial considerations. As you will see later, we believe the investment in the detector and the 20,000 channels needed to service it were about sufficient to make the physics unambiguous.

At Brookhaven, the Alternating Gradient Synchrotron accelerates protons to 28.3 GeV with a repetition rate of 1.4 s. The protons are extracted in a single turn and, after being transported from the machine area, strike a titanium target. Figure 6 shows a plan of the production area. At the target π and K mesons were made and focused into the decay region. A cylindrically symmetric conductor system carried a pulsed current of about a quarter of a million amps making a B-field that focused the charged particles into a parallel beam from the titanium target. The parallel beam passed down a shielded tunnel, and pions decayed primarily through the reaction

$$\pi \rightarrow \mu + \nu_\mu ,$$

to form a neutrino beam. Pions were focused in this system around 3 GeV/c and decayed to neutrinos at 1.2 GeV. The transverse momentum in the reaction is about 30 MeV/c so that the neutrinos emerged strongly peaked in the forward direction.

K mesons decay primarily through

$$K \rightarrow \mu + \nu_\mu ,$$

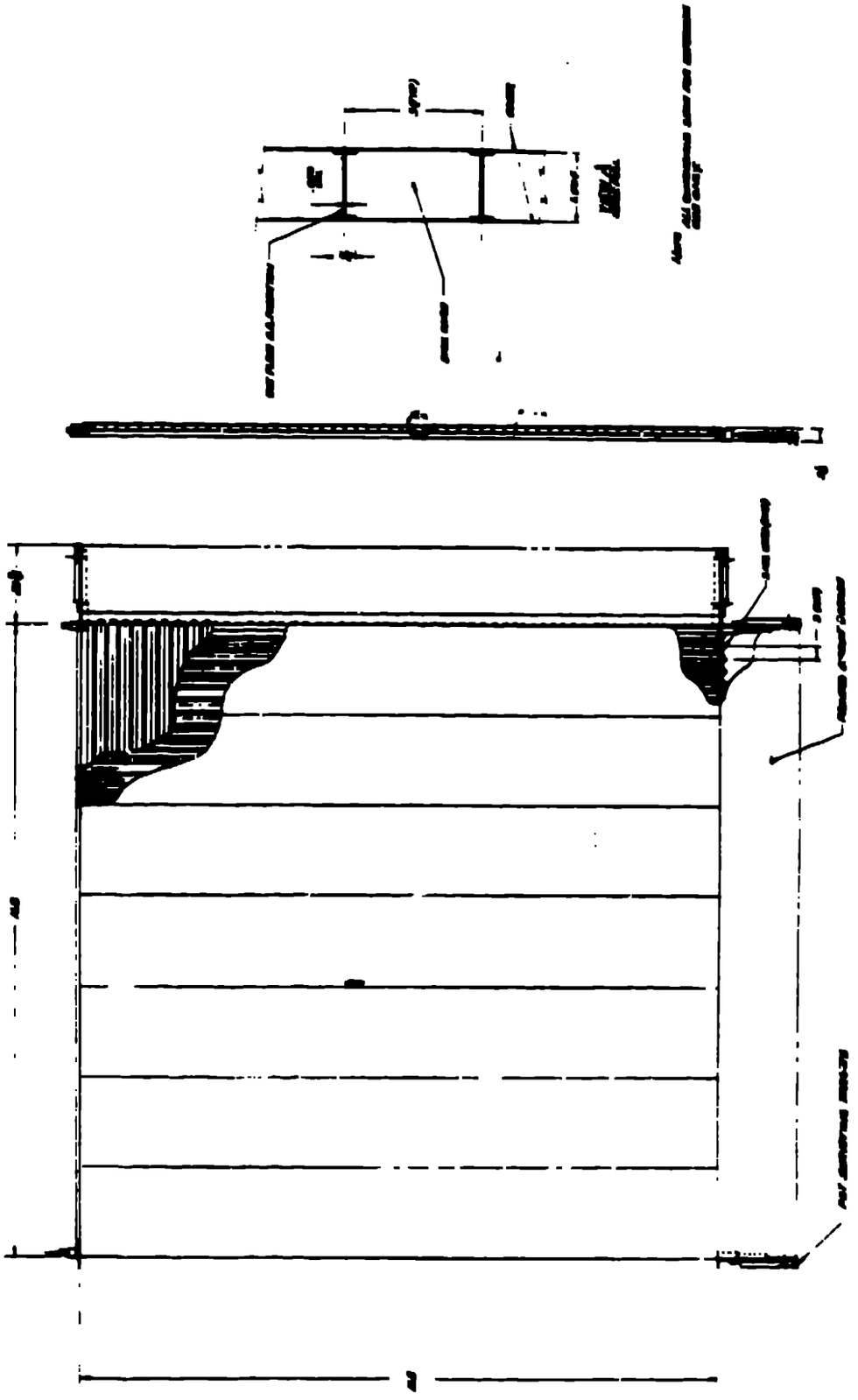

Figure 5

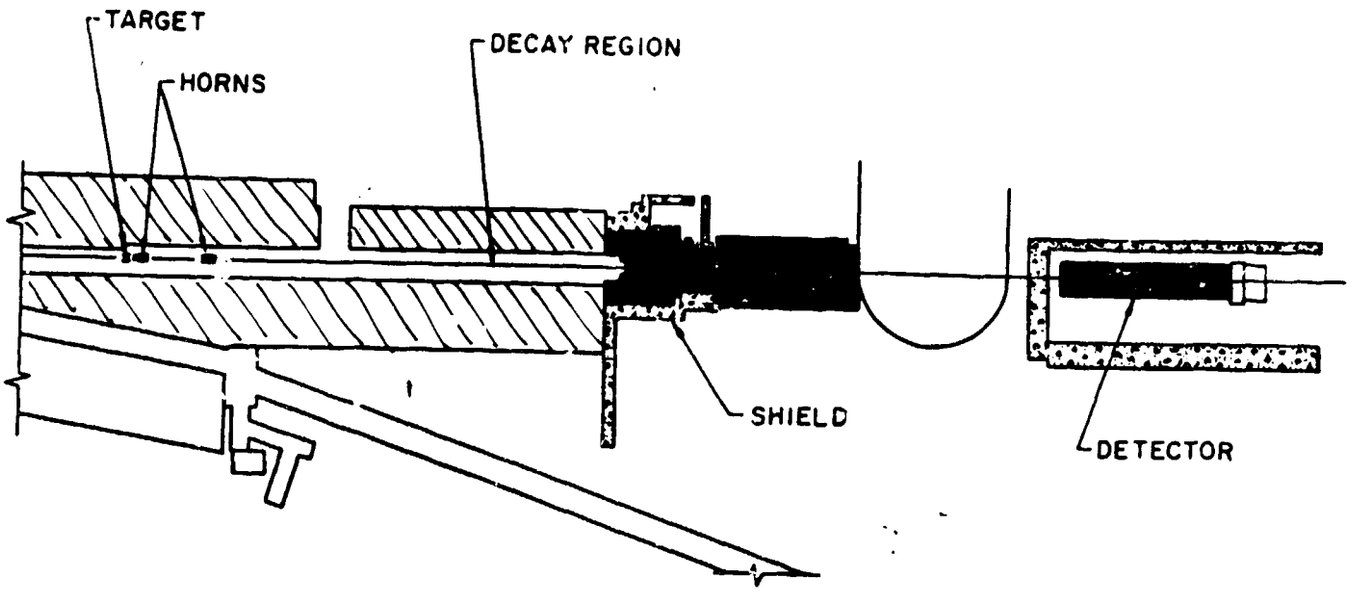

Figure 6

and although these neutrinos were somewhat more spread in angle, they contributed to the beam intensity in a different momentum region as we shall see later.

The neutrinos had a typical energy a little above 1 GeV and at an AGS intensity of more than 10^{13} per pulse there were about 10^{10} neutrinos passing through the detector. The beam was bunched by the accelerating radio frequency in the AGS so that there were twelve bunches 224 ns apart. The extraction process preserved this time structure, and the neutrinos also since the trajectories did not vary much in length from the target. This time structure was seen in the neutrino events as shown in Fig. 7. It is clear that background from neutrons for example was relatively small mostly because neutrons rattled around before they got to the detector because of the shielding and the few that were seen arrived late. Downstream of the decay region the proton beam was buried in a stop, and then an iron shield filtered out the remaining hadrons and muons from the particle decays. At the target the beam spectrum was as shown in Fig. 8. We shall return to a detailed discussion of this spectrum later.

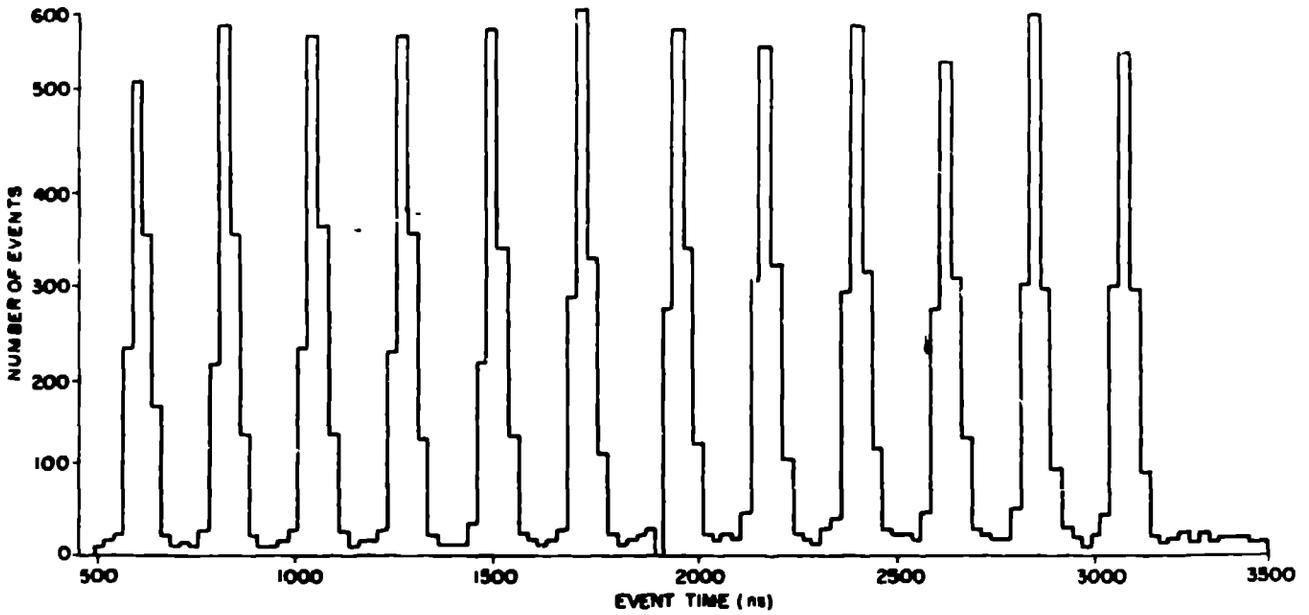

Figure 7

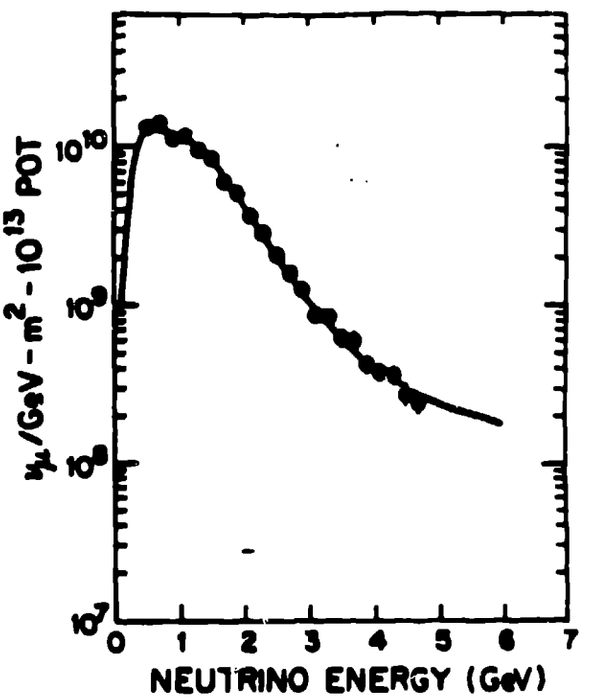

Figure 8

In the discussion of neutrino-electron scattering in the introduction, we specified that the signal for the reaction was a single electron in the forward direction. In Fig. 9 we show a candidate event. An electron generates a shower passing through material first by a bremsstrahlung process and then by pair production of the hard photon. So an electron at first looks like a minimum ionizing track–then, after a radiation length, produces a photon at a small angle and after another radiation length becomes three charged particles and goes on to the shower maximum. In this detector a radiation length was five modules thick, and since shower generation is a continuous business it leads to a typical event like that in Fig. 9. Part of the experimental process was the isolation of those events. Software was developed that recognized the fluctuating pattern characteristic of an electromagnetic shower, in contrast to the normal hadronic event in which tracks were well-defined and linear. This process yielded events that were real candidates for a single electromagnetic shower, and many events that satisfied fluctuation requirements in all kinds of aberrant ways. These events were removed by visual scanning of the data. After this process was

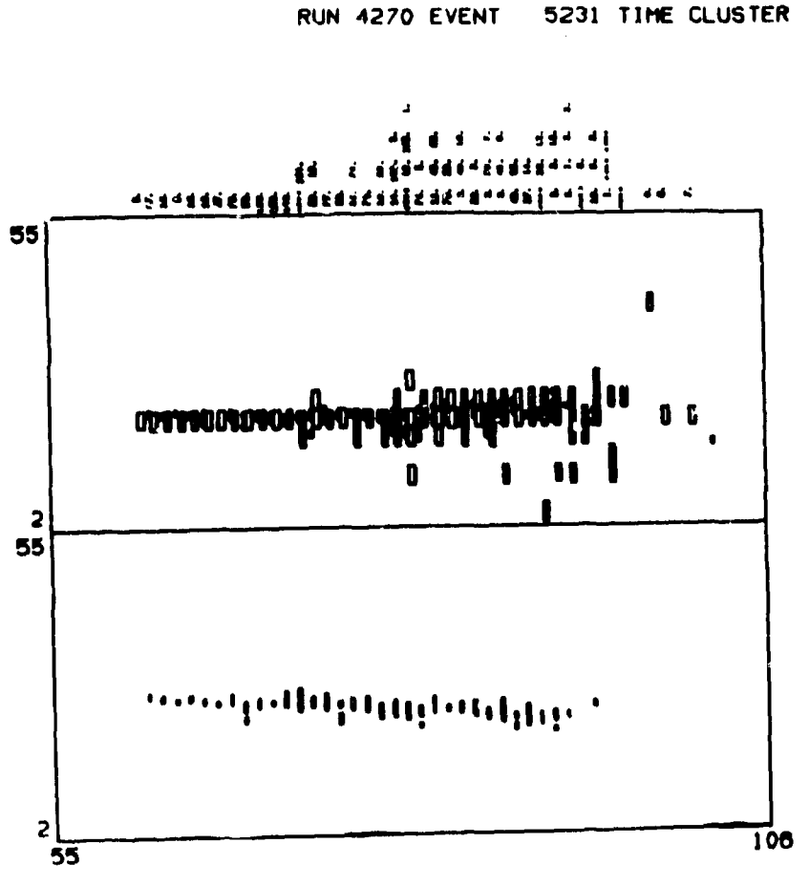

Figure 9

complete the time distribution of the events was as in Fig. 10. Note that there was no longer any background that was not correlated with the beam arrival time; neutron background was entirely removed.

The principal background after the selection for showers that were unaccompanied by anything else was from neutral-current reactions like

$$\nu_\mu + n \rightarrow \nu_\mu + n + \pi^0 \quad .$$

The π^0 decayed to two γ's right at the vertex, and often the second γ was lost out of the side of the detector. Then the remaining γ converted giving a single shower in the detector. Since this electromagnetic shower was formed from a gamma ray converting into an $e^+ e^-$ pair, the shower started off as twice minimum ionizing in contrast to the electron sample showers, which were singly minimum ionizing. In Fig. 11 are shown pulse-height distributions from a) minimum-ionizing particles, probably muons. In Fig. 11b are shown electrons from a test beam, and Fig. 11c shows gamma rays identified from the fact that the shower was accompanied by an upstream vertex and hence from a π^0 from a hadronic reaction. Figure 11d is the candidate sample, a mixture of gamma rays and electrons, as can be easily seen. In Fig. 12 is shown the energy loss from electrons in a test beam showing the correlation between the energy loss from the scintillator and in the PDT's and the cut, which was used to separate electrons from photons. This cut was 90% efficient in selecting electrons and reduced the photon contamination by about a factor of three.

Figure 13 shows the angular distribution of the electron candidate events with a clear peak in the forward direction, which was identified with neutrino-electron scattering. The distribution is plotted as a function of θ^2 because at small angles the solid angle is proportional to θ^2 and the background is expected to be flat in this variable. In Fig. 14 is shown a similar distribution for antineutrinos with the background components identified. Note the contamination of ν_e, wrong helicity neutrinos in the beam, and residual events from photons and misidentified hadrons. The importance of understanding the constituents in the background is emphasized by the contribution from ν_e-induced quasi-elastic scattering, which is not flat in contrast to the other backgrounds, because of Pauli suppression at low Q^2.

There is no direct way to count the number of incident neutrinos corresponding to the sample of neutrino-electron scattering events that have been isolated as described above. The method that is chosen to normalize the cross section relies on selecting a sample of events in the same run in which the cross section is known. Such a reaction is quasi-elastic scattering

$$\nu_\mu + n \rightarrow \mu^- + p$$

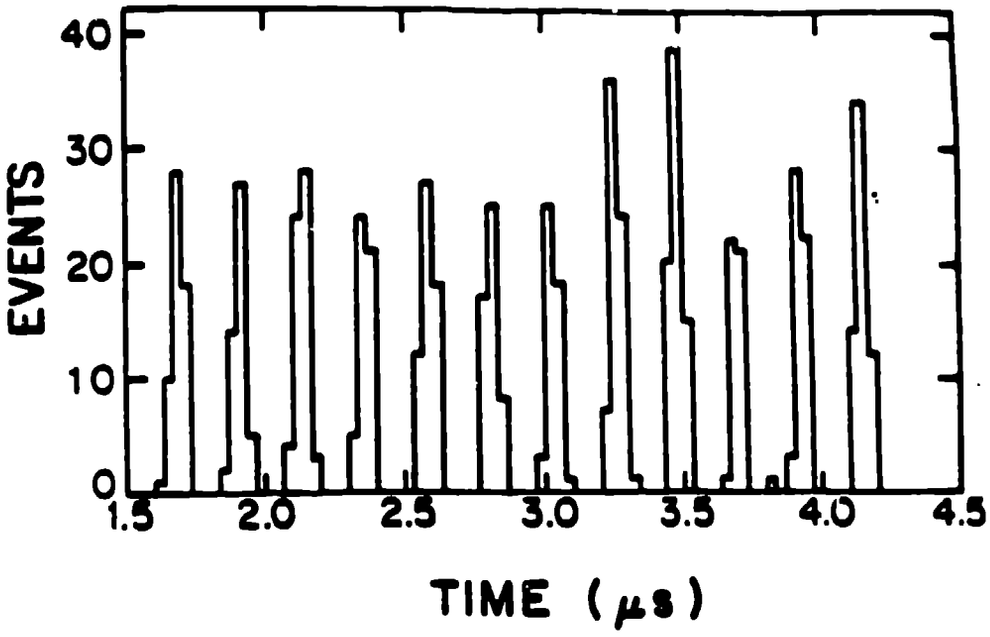
EVENTS
40
30
20
10
0
1.5
2.0
2.5
3.0
3.5
4.0
4.5
TIME (μs)

Figure 10

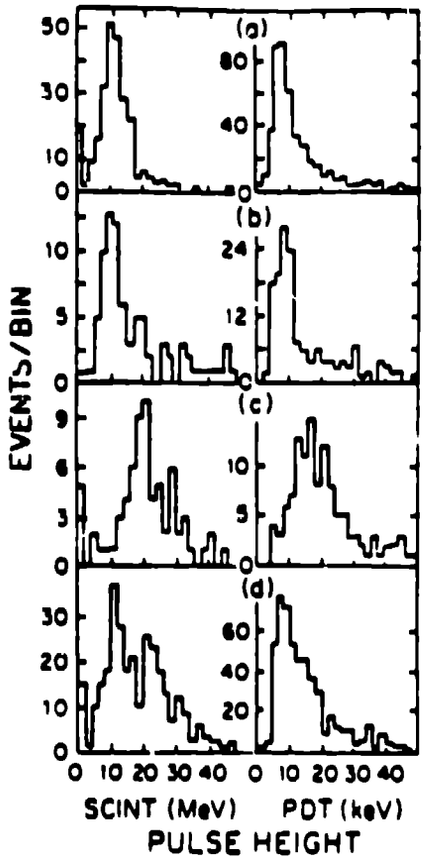
EVENTS/BIN
(a)
(b)
(c)
(d)
0 10 20 30 40
0 10 20 30 40
SCINT (MeV)
PDT (keV)
PULSE HEIGHT

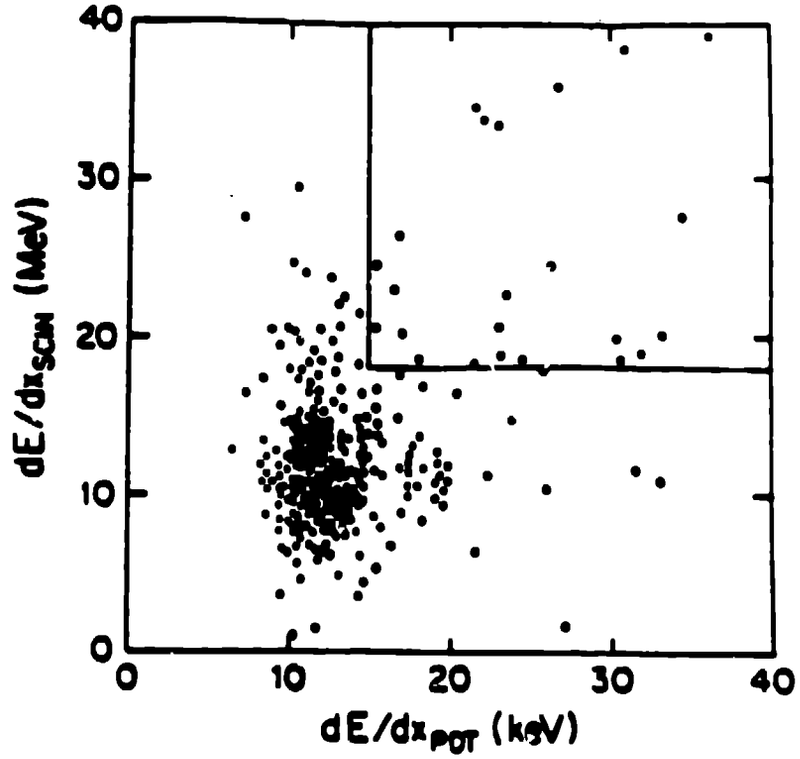

Figure 12

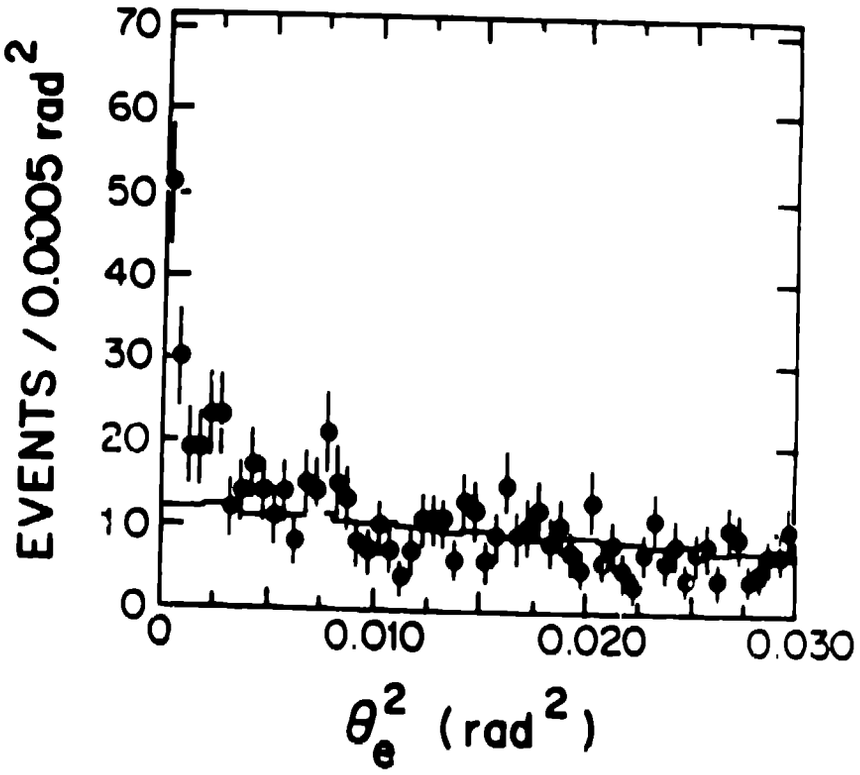

Figure 13

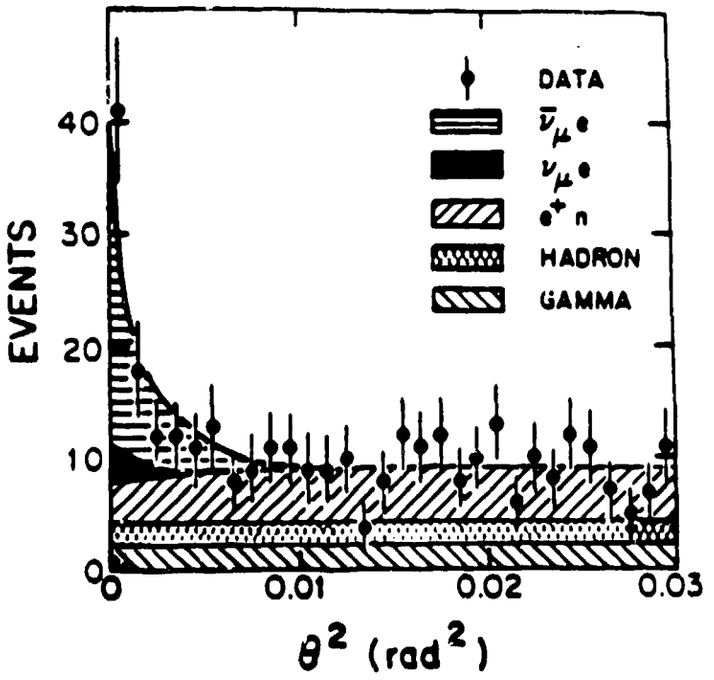

Figure 14

or

$$\bar{\nu}_\mu + p \rightarrow \mu^+ + n \ .$$

The cross section is known from knowledge of the charged-current coupling constant G_F. It remains to understand the form factors appropriate to the nucleon. The vector form factor is carried over from electron scattering using CVC and a similar form is used for the axial current with M_A instead of M_V in a dipole parameterization. The event sample is selected by choosing events in which the muon is within 20° of the neutrino direction so that the recoil particle is low enough in energy so that no track is formed in the detector. In addition, other activity in cells of the detector is limited so that inelastic events are discriminated against. It remains to average the cross section within a polar angle of 20° over the calculated neutrino spectrum to complete normalization. A feature of this method is that the cross sections for neutrino-electron scattering and quasi-elastic scattering within a fixed angle are both proportional to the neutrino energy in this energy and angle range. The effect of this proportionality is that, in first order, errors in knowledge of the shape of the spectrum cancel in the normalization process. Apart from Pauli suppression at very small angles, the effect of having the nucleon target in a nucleus (^{12}C) is negligible. Moreover because the experimental method relies on a measurement of the ratio of the cross sections for neutrino and antineutrino scattering a further cancellation of systematic errors occurs. The systematic errors of the ratio of the cross sections are shown in Table I.

Table I. Contributions to systematic errors in cross-section determination.

Component	*Uncertainty in R*
M_A	1%
Acceptances	4%
Single pion cross sections	5%
Multi pion cross sections	5%
Tracking and event selection	3%
Neutrino Flux	3%

The limiting errors stem from the knowledge of the inelastic cross sections.

Although the agreement with the standard model is so compelling it is tempting to express the results of the experiment in terms of $\sin^2\theta_W$, it is possible to perform an analysis in terms of g_A and g_V in a model-independent way. The result of this analysis is shown in Fig. 15 where each cross section limits the values in the g_A–g_V plane to an ellipse. The intersection of these ellipses gives for one solution a small value of g_V and g_A, close to -1/2, of course in agreement with the standard model.

In Fig. 16 is shown the kinematic limit for the angle of the electron in neutrino-electron scattering together with the measured angular resolution as a function of the electron energy. Knowing the angle and energy of the electron is sufficient to deduce the energy of the neutrino and so to calculate the value of the kinematic variable $y = E_e/E_\nu$. In our case the information from the angle is not sufficient to make a kinematic fit, but using the limited information it is possible to perform a model-independent analysis using the angular information. This analysis results in the breaking of the elliptical ambiguity as shown in Fig. 17. The preferred solution is again chosen by this analysis.

In summary, the cross-section results are shown in Table II, and a historical slide of the measurements of these cross sections with time is shown in Fig. 18. The value of $\sin^2\theta_W$ is in agreement with the world average of other determinations after radiative corrections at the one-loop level have been included, and so the standard model emerges unscathed by this encounter. A test that can be made with these data is that of the charged radius of the neutrino. Even though the charge of the neutrino is zero, a dipole moment would manifest itself in an extra contribution to the cross section through electromagnetic effects. This cross section would be enhanced by a 1/E addition in electron energy to the weak cross section and the total cross section for scattering above the electron energy threshold

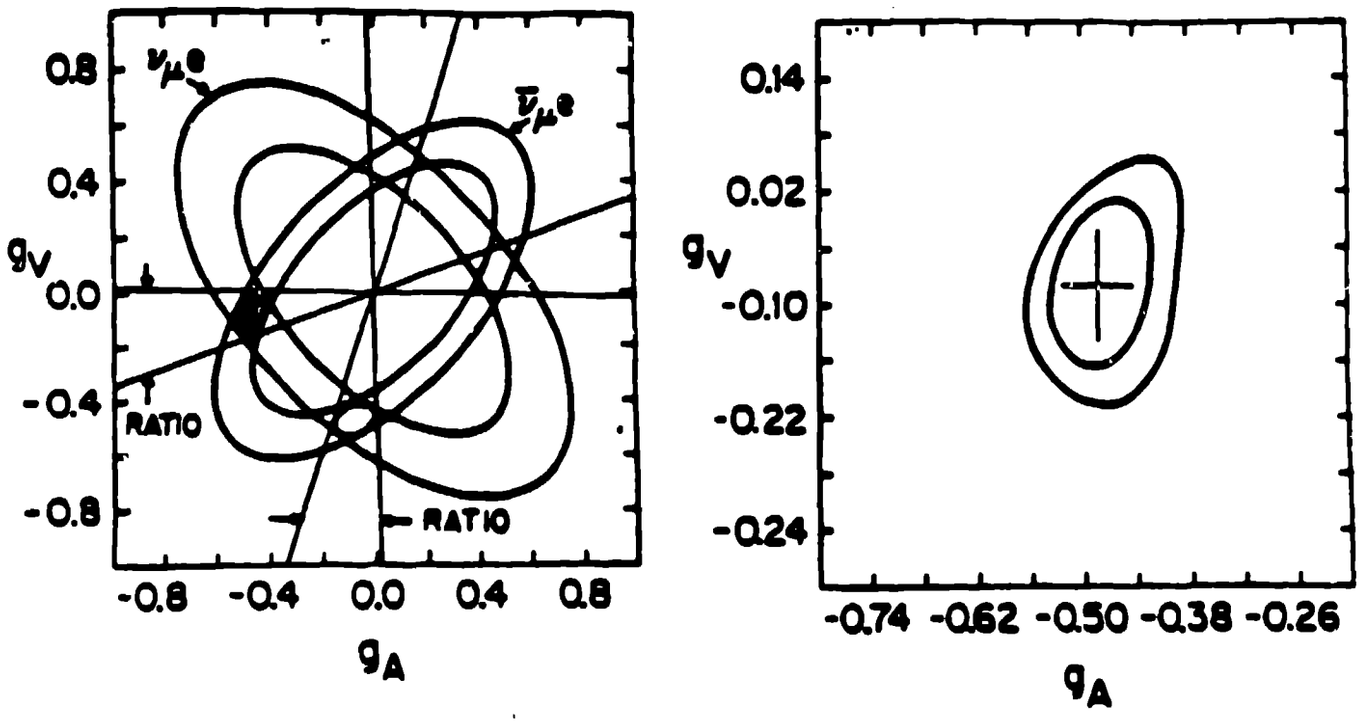

Figure 15

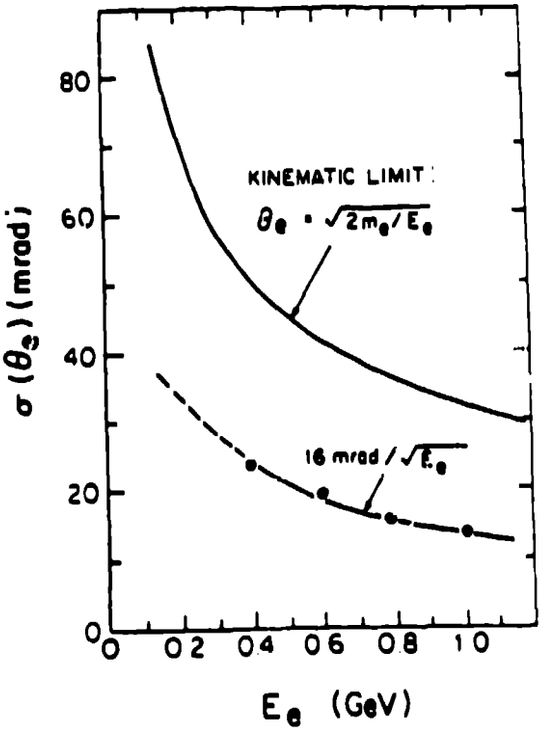

Figure 16

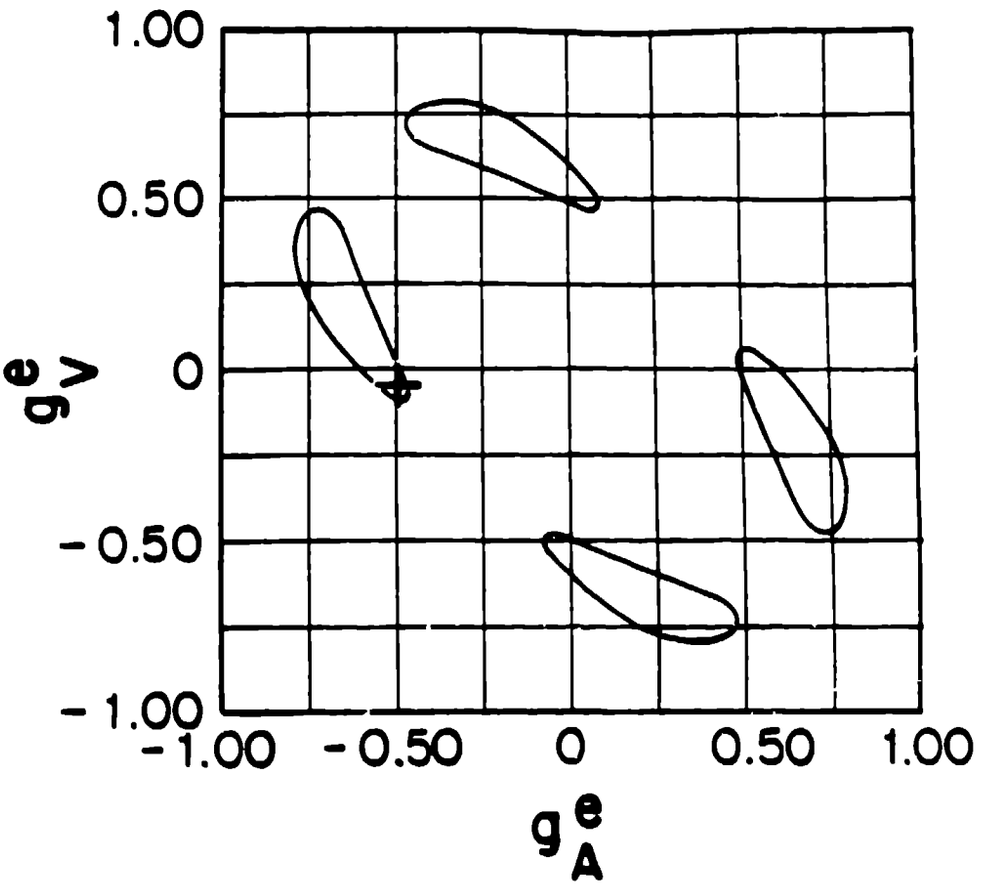

Figure 17

Table II

$\nu_\mu e \to \nu_\mu e$ elastic scattering

$R_e = \sigma(\nu_\mu e \to \nu_\mu e)/\sigma(\bar{\nu}_\mu e \to \bar{\nu}_\mu e)$

$1.38^{+0.40}_{-0.31}$

$\Rightarrow \sin^2\theta_W = 0.215 \pm 0.032\ (\text{stat}) \pm 0.012\ (\text{sys})$

$\sigma(\nu_\mu e \to \nu_\mu e)/E_\nu$

$1.85 \pm 0.25 \pm 0.27 \cdot 10^{-42}\ \text{cm}^2/\text{GeV}$

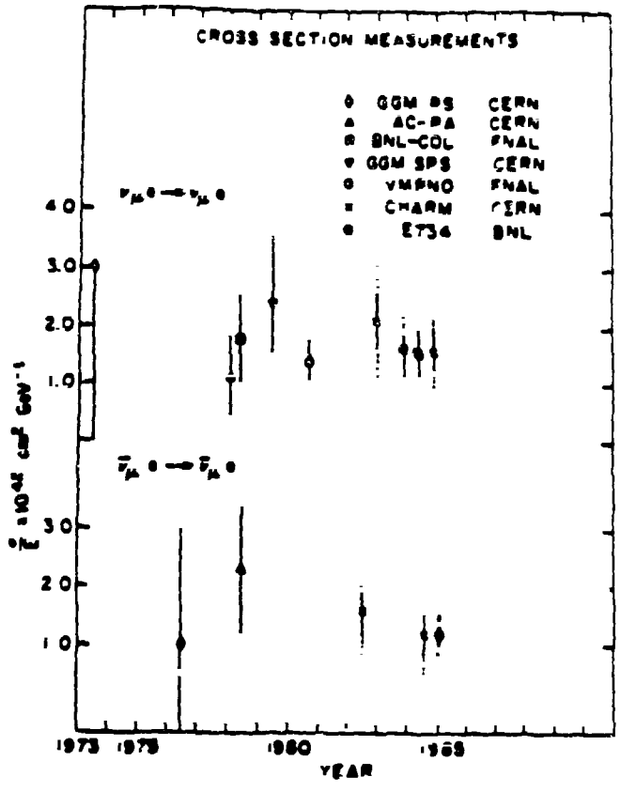

Figure 18

would be affected. Conversely, the agreement with the standard model puts a limit on the additional contribution, this limit is

$$< r^2 > \quad < 0.86 \times 10^{-32} \ .$$

It is worth noting that this demonstration of the point like electromagnetic character of the neutrino is comparable with that from scattering of charged leptons.

NEUTRINO-PROTON ELASTIC SCATTERING

$$\nu_\mu \ p \ \rightarrow \ \nu_\mu \ p$$

Neutrino-proton scattering is factorizable into coupling of the neutrino to the Z^0 and the coupling of the Z^0 to the proton. The proton is described by the quark model and so, of course, the Z^0 actually couples to the quark constituents. The hadron current is divided conventionally into vector and axial-vector parts. The vector part is related by CVC with the scattering of electrons from protons, which is empirically well understood. A parameterization due to Sakurai is used frequently to describe exclusive scattering of

neutrinos from nuclei where the amplitude is divided into weak isospin I = 1 and I = 0 parts. The vector part is

$$\alpha V_\mu(I=1) + \gamma V_\mu(I=0)$$

and the axial vector part

$$\beta A_\mu(I=1) + \delta A_\mu(I=0) \quad .$$

In the standard model,

$$\alpha = 1 - 2\sin^2\theta_W$$

$$\gamma = -2/3\sin^2\theta_W$$

$$\beta = 1$$

$$\delta = 0 \quad .$$

The expression for δ is of particular interest. It arises from the fact that the axial vector coupling is $\pm 1/2$ for both constituents of a family and in the approximation that the masses are not important, the contributions of the two quarks will cancel. In the case of the heavy quarks s, c in the sea, the masses of the quarks are very different and this cancellation will not be fully effective. It is of interest to try to detect a non-zero δ then.

At finite momentum transfers, the nucleon will exhibit a form factor that will affect the scattering amplitude. In electron scattering this form factor is represented empirically by the relation

$$\frac{1}{(1+Q^2/m_V^2)^2} \quad .$$

This expression is referred to as the dipole fit (at least in the old days). m_V represents the sum of the contributions of the vector mesons weighted by their relative coupling to the Z^0 and to the nucleon. Using this success for guidance it is conventional to parameterize the axial part in a similar manner

$$G_A = \frac{g_A(0)}{(1+Q^2/m_A^2)^2} \quad .$$

The coefficient g_A is extracted from neutron β decay (1.262 ± 0.005) and from charged-current reactions e.g.,

$$\nu_\mu + n \rightarrow \mu + p$$

with

$$m_A = 1.032 \pm 0.036 \quad .$$

Then the cross section for elastic scattering is with $s - u = 4m_p E_\nu - Q^2$

$$A = \frac{Q^2}{M_p^2}\left[G_A^2\left(1 + \frac{Q^2}{4M_p^2}\right) - F_1^2\left(1 - \frac{Q^2}{4M_p^2}\right)\right.$$
$$\left. + F_2^2\left(1 - \frac{Q^2}{4M_p^2}\right)\frac{Q^2}{4M_p^2} + F_1 F_2 \frac{Q^2}{M_p^2}\right] \quad ,$$
$$B = \frac{Q^2}{M_p^2} G_A(F_1 + F_2) \quad ,$$
$$C = \frac{1}{4}\left(G_A^2 + F_1^2 + F_2^2 \frac{Q^2}{4M_p^2}\right) \quad .$$

F1 and F2 are functions of Q^2, m_V^2 and the anomalous magnetic moments of the proton and neutron. C is relatively flat; B grows also with Q^2. This illustrates the difference between neutrino and antineutrino scattering, because the sign in front of the B term changes sign, accounting for the fact that antineutrino-proton scattering has a steeper Q^2 dependence than neutrino scattering.

A typical event is shown in Fig. 19. Neither incident nor outgoing neutrinos are seen and only the recoil proton is visible. The energy of the proton is proportional to Q^2 which varies up to $Q^2 = 1$ GeV. It is a nice experimental trick that if protons are selected that stop in the detector, then by swimming up the proton backwards from the stopping point, all protons look the same apart from their track length. In this way the proton can be differentiated from pions and electrons without reference to their energy. In fact after the particle is identified, the energy is known and hence also Q2. The difficulty with this experiment rests on two facts. First, most of the protons are bound in nuclei, ^{12}C. Not only are these protons bound but they may scatter or even charge exchange on the way out of the nucleus even though ^{12}C is a small nucleus. Corrections must be made for these effects, and account must be taken of the fact that other relatively weakly correlated nucleons will come out leaving energy deposited in the detector. This energy occasionally confuses the analysis resulting in the event being lost. Recoil protons of high energy can also interact in the body of the detector so that the s rent energy is reduced or the kink in the track again causes the event to be lost in analysis. In short, the range of Q^2 that can be analysed reliably is limited at the low end by track length and rescattering and at the high end by interaction of high-energy protons in the detector material. Of course a lot of effort is expended in understanding these effects and correcting for them until a cross section like that plotted in Fig. 20 is generated. The cross section is averaged over the

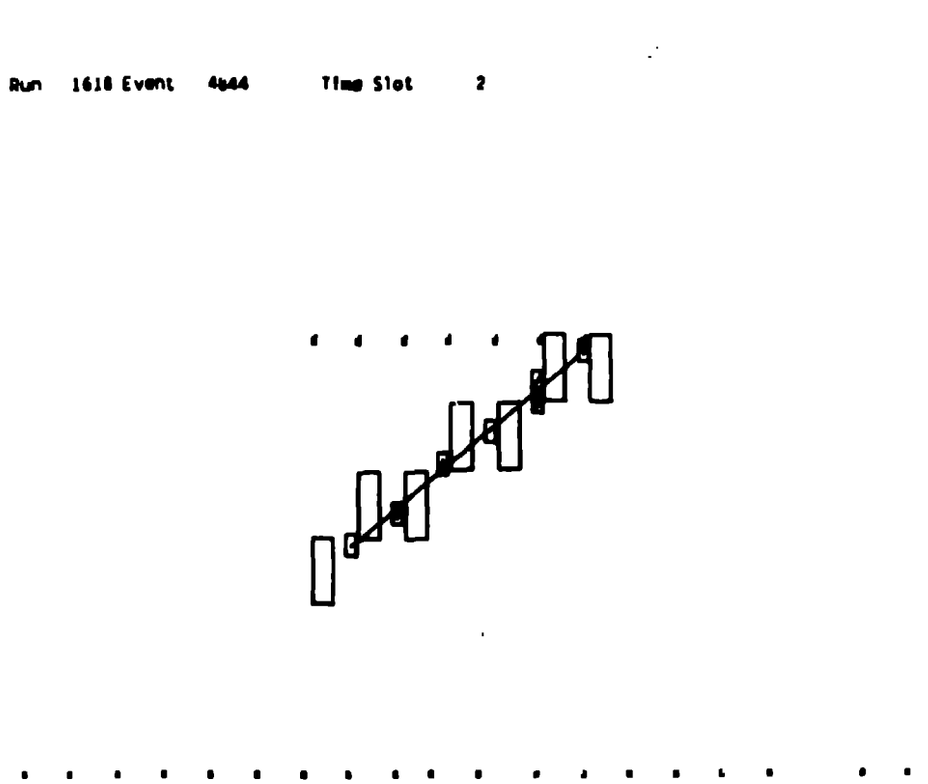

Figure 19

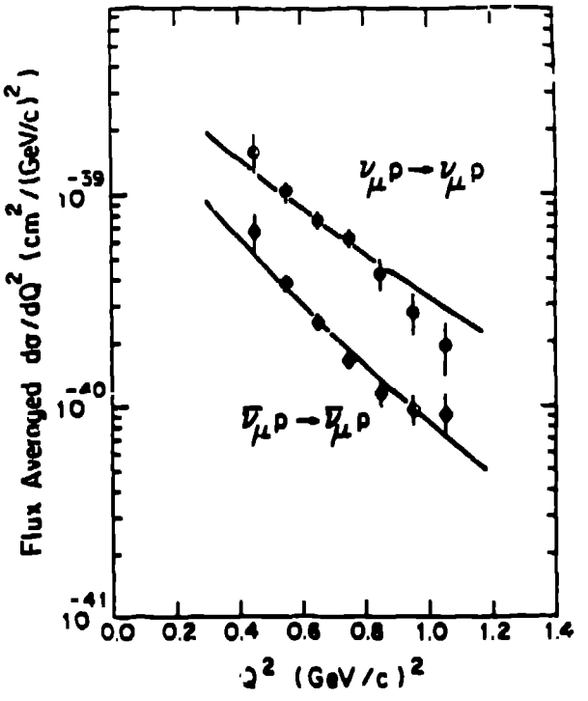

Figure 20

incident neutrino spectrum, which is used in the Monte Carlo leading to the theoretical fits in the same Figure. Quasi-elastic scattering is used to provide a normalizing reaction in much the same way as in the neutrino-electron scattering experiment.

In Table III is shown the ratio of neutrino-proton neutral-current scattering to quasi-elastic scattering as well as the same ratio for antineutrinos. From these ratios a value for $\sin^2\theta_W$ is extracted, and even though the systematic errors are a little large, the value for $\sin^2\theta_W$ is in agreement with other determinations, notably in neutrino-electron scattering.

In the standard-model expression for the coupling constants above, it was stated that δ, the axial vector I = 0 coupling constant, was zero. The reason that δ is zero is that there are contributions from both elements of a weak quark doublet and these contributions are equal and opposite and cancel, at least in the approximation that the masses are irrelevant. This is fine for u and d quarks but much less so for s and c. The masses of s and c are very different so that the cancellation is not expected to be complete. The magnitude of the effect is uncertain partly because of the uncertainty of the heavy-quark content of the sea and partly because this is a sublety of QCD and not so well calculable. It would be interesting therefore to measure this quantity as an aid and service to theorists. Failing more detailed guidance it is assumed that the Q^2 dependence of this contribution will be the same as the other axial vector form factor and described by m_A and a dipole fit.

Table III

$\nu_\mu p \rightarrow \nu_\mu p$ elastic scattering

$$R_\nu = \sigma(\nu_\mu p \rightarrow \nu_\mu p)/\sigma(\nu_\mu n \rightarrow \mu^- p)$$
$$= 0.153 \pm 0.007\ (\text{stat}) \pm 0.017$$
$$R_\nu = \sigma(\bar{\nu}_\mu p \rightarrow \bar{\nu}_\mu p)/\sigma(\bar{\nu}_\mu p \rightarrow \mu^+ n)$$
$$= 0.218 \pm 0.008\ (\text{stat}) \pm 0.023$$
$$\sin^2\theta_W = 0.220 \pm 0.016\ (\text{stat}) \begin{smallmatrix}+0.023\\-0.031\end{smallmatrix}\ (\text{sys})$$

Axial Isoscalar Contribution

$$\epsilon = 0.12 \pm 0.07$$

Then, since the coefficent of the axial-vector form factor is known from neutron decay very precisely when only u and d quarks participate, it is possible to fit for a different coefficient in the measured cross section. Indeed this was done and a value for $(1 + \epsilon)$ enhancing $g_A(0)$ was obtained and shown in Table IV. It is barely significant but in agreement approximately with theoretical estimates in the literature. It would be nice to do better, but it is a hard experiment because of the nuclear effects in the target, as we have discussed above.

NEUTRINO OSCILLATIONS.

The possibility that mixing between neutrino flavors may occur accounts for the continuing experimental search for neutrino oscillations. If there is such mixing, and the neutrinos have a different mass, then the two mass eigenstates may acquire a phase difference in flight and so the weak eigenstates can vary along the beam. Experimentally, the most sensitive searches occur when an initially pure beam is measured by observing flavor-sensitive interactions. At an accelerator, pions are produced copiously and the decay $\pi \rightarrow \mu + \nu_\mu$ produces the main component of the neutrino beam. Some ν_μ are produced from K decay, from

$$\begin{aligned} K &\rightarrow \mu + \nu_\mu \\ &\rightarrow \mu + \nu_\mu + \pi^0 \quad . \end{aligned}$$

Although ν_e are produced rarely in a high energy accelerator beam, they are certainly present and the main decay modes are

$$\begin{aligned} \mu &\rightarrow e + \nu_e + \bar{\nu}_\mu \\ K &\rightarrow \pi^0 + e + \nu_e \quad . \end{aligned}$$

The natural ν_e are a little less than 1% of the ν_μ and the most sensitive accelerator oscillation searches are usually for $\nu_\mu \rightarrow \nu_e$. The probability of finding ν_e in a pure ν_μ beam is

$$P = \sin^2 2\alpha \ \sin^2(1.27\Delta m^2 \ell / E_\nu) \quad .$$

The sensitivity of the experiments is limited to a fraction of the expected ν_e contamination, depending on statistics and the confidence of the experimenter in calculating the naturally occurring background. In recent years the dependability of calculations of neutrino flux has improved and now is good to better than 10% of the absolute flux. In Fig. 21 is shown the ν_μ flux for the BNL broad-band beam with the partial contributions from p and K decay. In Fig. 22 is shown the ν_e flux from the same calculation together with the major

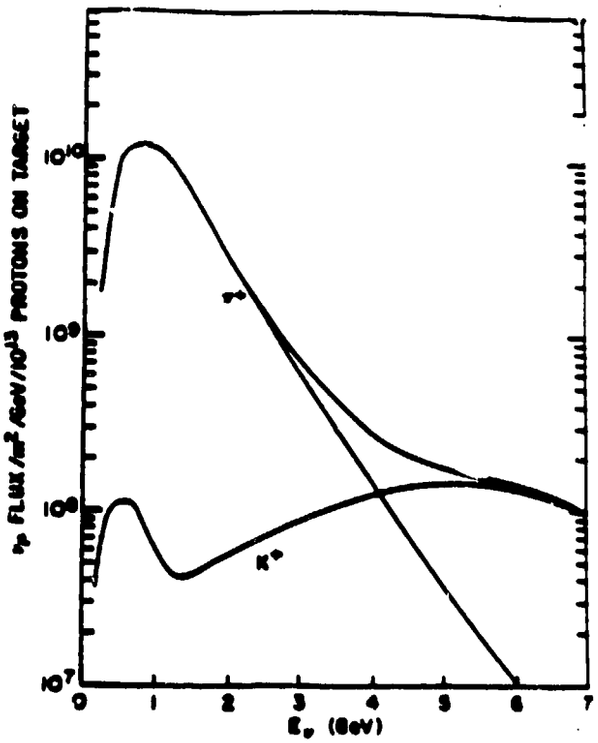

Figure 21

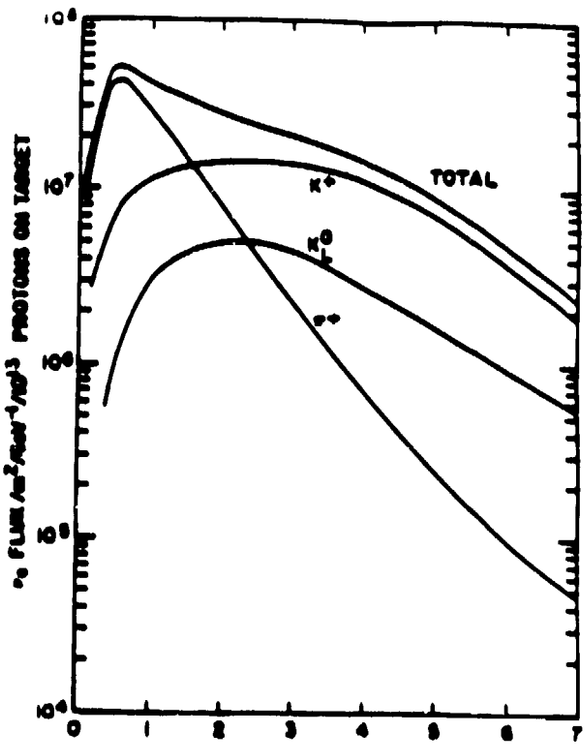

Figure 22

contributions from p and K decay. The principal uncertainty in these calculations is in estimating the complex particle production processes in the target where there is the possibility that the incident proton may interact more than once, as may the outgoing pion. A felicitous experimental situation occurs when the only ratio of ν_μ to ν_e is involved, namely, that the effect of the initial processes tends to cancel. For oscillation limits then, the ratio of the naturally occurring neutrinos is well known even as a function of energy.

In the BNL experiment that we have discussed at length, the apparatus is designed to identify electrons and to measure their energy. Electromagnetic showers have been identified and they are plotted as a function of the observed energy in Fig. 23. A remaining experimental problem is to separate photon-induced electromagnetic showers from electron-induced ones. The method that was used in the neutrino-electron scattering experiment will not work because the recoil proton confuses the identifying algorithm at the front of the track. By looking for upstream activity in the event, a way of identifying the photon induced showers emerged. If there were such energy deposition in the event, then the shower could only occur from a secondary interaction so that it was reasonably certain that events with upstream activity were photon-induced showers from π^0 decay. The energy distribution of all showers is shown in Fig. 24a, and the "photon" showers in Fig. 24b. Since there are very few electrons below 1 GeV, these distributions can be normalized to one another below 1 GeV and a subtraction of the combination from photon showers made. The electron distribution is shown in Fig. 24c. In Fig. 23 is shown the electron-neutrino spectrum as a function of energy, together with the result for the expected ν_e flux. After comparing this electron distribution with the ν_μ spectrum of Fig. 8, a limit for the contribution of oscillations to the ν_e spectrum can be made and at 90% confidence, it is shown in Fig. 25. This might be the end of the story but for two more results that have been talked about extensively. The first result comes from experiment PS 191 at CERN in which a search was made for events that had electrons coming from a vertex defined by another track. In Fig. 26a is shown a normal neutrino interaction in this apparatus. Fig. 26b shows an interaction in which an electromagnetic shower apparently emerges from the vertex directly. Such an event can only be produced by an induced-charged-current interaction from the residual ν_e in the beam or by a photon from a π^0 converting so close to the vertex that it is mistaken for an electron. To separate these fake events a plot is made of the conversion distance of the showers. This plot for PS 191 is shown in Fig. 27 where a clear excess is shown at small distances. This number of events is far too many to be accounted for by normal ν_e in the beam and it has been speculated that this is because of neutrino oscillations producing more ν_e than expected. Without going into too many

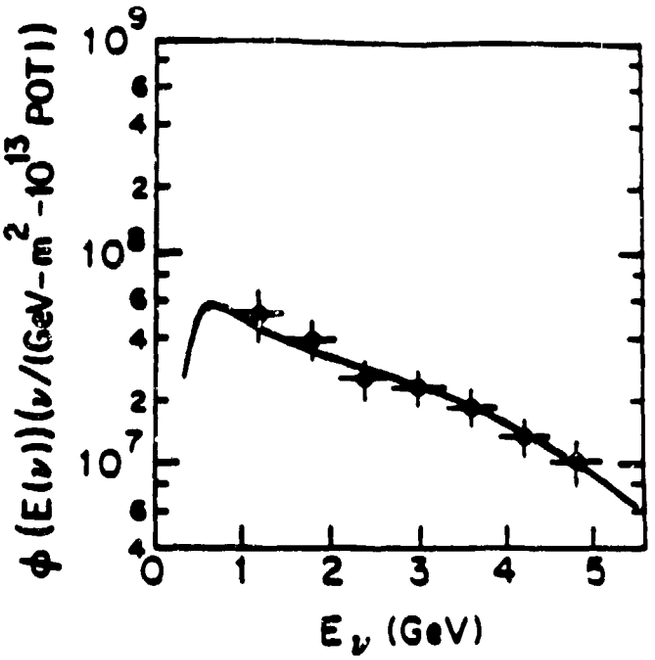

Figure 23

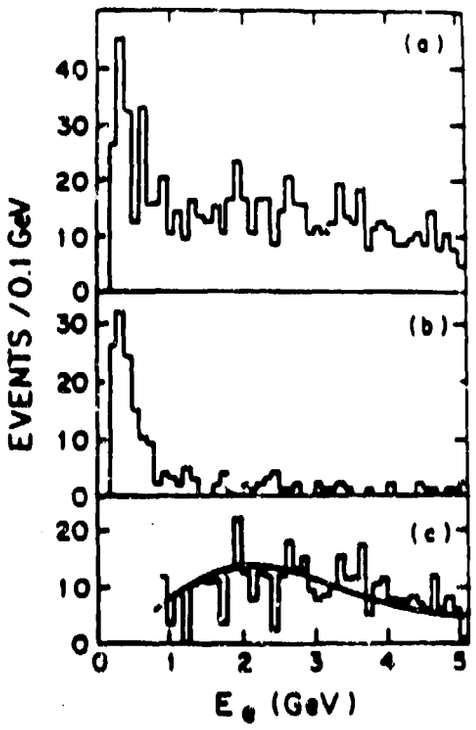

Figure 24

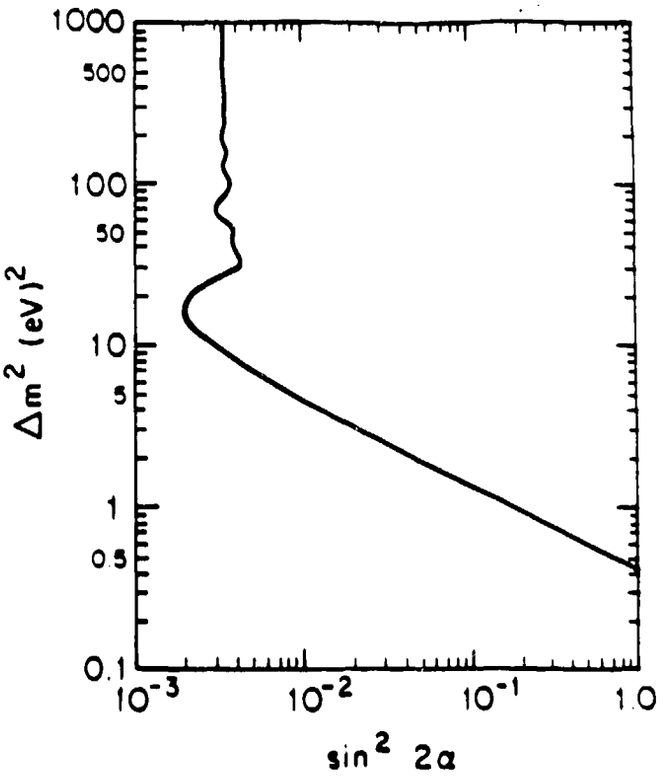

Figure 25

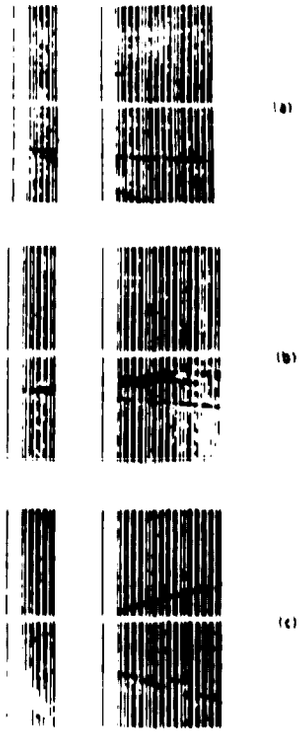

Figure 26

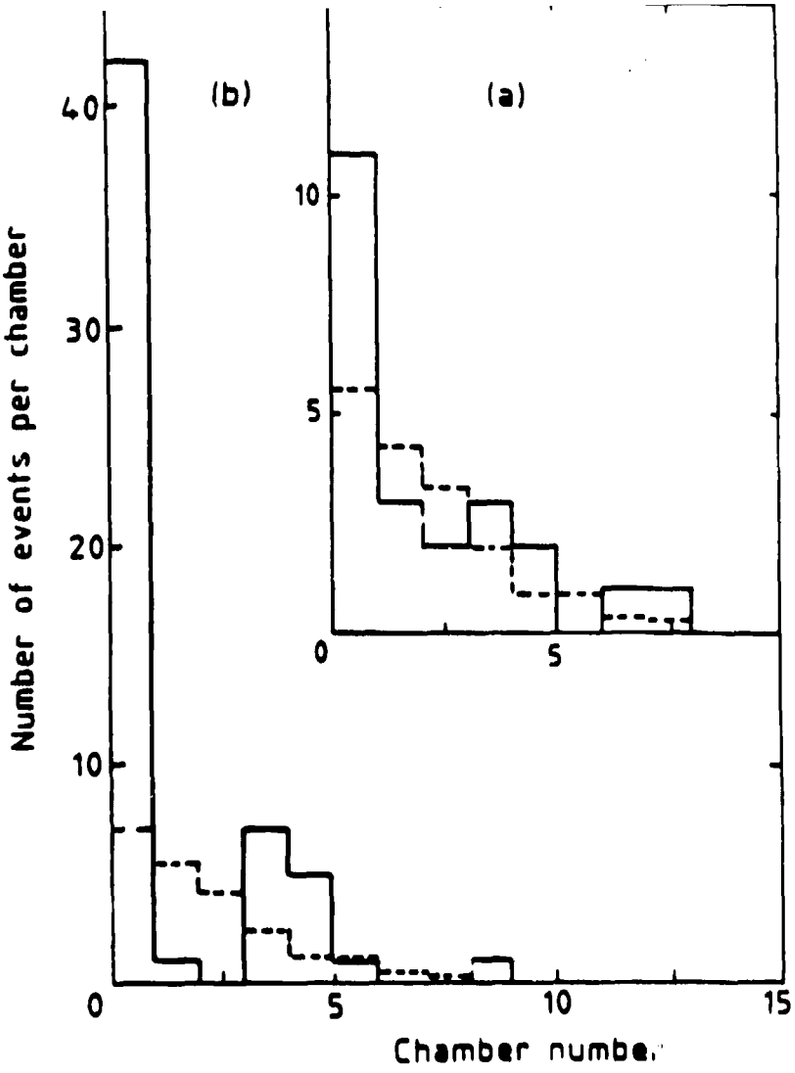

Figure 27

details let it be said that the oscillation limit described above for E734 is in contradiction with this measurement. In fact an almost similar measurement made in E734 is shown in Fig. 28 where no copious signal is seen. Cuts on the data are somewhat different in the two cases and with ingenuity a scenario can be invented to escape experimental confrontation. Adding to the confusion is an experiment also performed at BNL where a similar detector is placed about a kilometer away (CIJH), shown in Fig. 29. This experiment sees too many electrons for conventional explanation. No single phenomenon can explain all these observations, and a great deal of discussion has ensued, some of it heated. Since most of this talk has focused on verification of the standard model in detail it seemed amusing to focus at the end of this talk on an area where confusion reigns. I can only urge you to follow the literature and see how it all comes out. Without massive prejudice, the score cannot be called at this time.

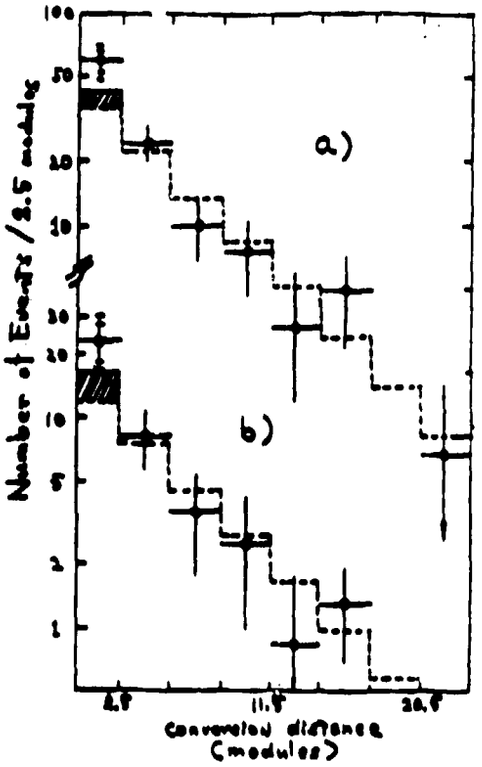

Figure 28

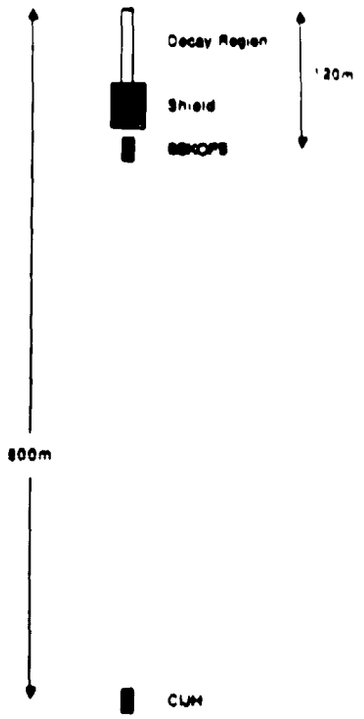

Figure 29